Available online at www.sciencedirect.com

ScienceDirect

Procedia Engineering 64 (2013) 1552 – 1561

Procedia Engineering

www.elsevier.com/locate/procedia

International Conference On DESIGN AND MANUFACTURING, IConDM 2013

3D Heterogeneous multi-sensor global registration

Joaquín Rivero-Juárez[a], Edgar A. Martínez-García[a,]*, Abril Torres-Mendez[b], Rajesh E. Mohan[c]

[a]*Laboratorio de Robótica, Institute of Engineering and Technology*
Universidad Autónoma de Cd. Juárez, Ave. del Charro 450 Norte, Juárez, Chih., 32310, MEXICO.
[b]*CINVESTAV Campus Saltillo, Ramos Arizpe, Coahuila, MEXICO*
[c]*Singapore University of Technology and Design, 20 Dover Drive, Singapore, 138682, SINGAPORE*

Abstract

This manuscript presents a deterministic model to register heterogeneous 3D data arising from a ring of eight ultrasonic sonar, one high data density LiDAR (light detection and ranging), and a semi-ring of three visual sensors. The three visual sensors are arranged in a cylindrical ring, and although they provide 2D colour images, a radial multi-stereo geometric model is proposed to yield 3D data. All deployed sensors are geometrically placed on-board a wheeled mobile robot platform, and data registration is carried out navigating indoors. The sensor devices in discussion are coordinated and synchronized by a home-made distributed sensor suite system. Mathematical deterministic formulation for data registration is used to obtain experimental and numerical results on global mapping. Data registration relies on a geometric model to compute depth information from a semi-circular trinocular stereo sensor that is proposed to rectify and calibrate three image frames with different orientations and positions, but with same projection point.

Keywords: data registration; sensor suite; sensing model.

1. Introduction

Mobile robots need accurate information about its environment to achieve useful tasks such as path-planning, autonomous navigation, robot localization, mapping and so forth. Sensor fusion is an engineering research field of study about the process to combine measurements from different sensors, or single sensor with spatio-temporal frames to provide a robust and a complete description about environmental objects [8]. Sensor fusion is used to

* Corresponding author. Tel.: +52-656-688-4843; fax: +0-000-000-0000 .
E-mail address: edmartin@uacj.mx

doi:10.1016/j.proeng.2013.09.237

yield sensor redundancy in order to reduce uncertainty of measurements [11-12], to improve the perception of the world in order to take smart decisions [1]. Data registration is a field that search for models to accurately store data obtained from sensors at different spatio-temporal sensor measurements. Thus, 3D heterogeneous data refers to depth information arising from different types of sensors, and/or a diversity of sensing modalities. The discussion in this paper concerns formulation on data registration to combine three sensing models on-board a mobile robot. Sonar and LiDAR sensors are active and its modality is range, while radial multi-stereo is passive and its modality is vision. 3D data could be represented by point sets, planes, triangulated surfaces, 3-D lines and voxels. However, our focus in this paper is the proposal of a deterministic model scoping on-line registration of exteroceptive heterogeneous 3D data. The research problem is how to establish a general mathematical model to store rich datasets for 12 sensors of 3 types, and different sensing modalities. The manuscript is organized as follows: Section 2 describes the architecture of a sensor suite system. Section 3 describes the robotic platform and the kinematic model. Section 4 and 5 describe the sensing models for a ring of ultrasonic sonar, and a laser range finding sensor, respectively. Section 6 describes the proposed sensing model for a radial multi-stereo system. Section 7 presents experimental results, and finally the Conclusions are given to summarize our findings.

2. Distributed Sensor Suite

A sensors suite (SS) is a device comprised of multiple interconnected sensors that are controlled, coordinated, and synchronized to accomplish detection of relevant environmental percepts through information synthesis [3-4]. Since it manages sensors with different kind of transducers, the types of energies are also diverse. Therefore, a SS provides distinct sensing modalities, and it is purposed to obtain reliable information through physical and logical redundancy [2]. In the present research work we are deploying a home-made apparatus with a distributed computer system for data registration (see fig. 1 left and center). The sensor devices instrumenting the SS are concretely summarised in table 1 classified by their data types. We established a sensor device identifier namely ID, and their symbolic variables that represent the types of data.

Table 1. Sensor suite devices & types of data.

Sensor	ID	Modality	Type	Variable
Stereo Vision	S1	Vision / range	Pasive	$P=(x,y,z)^{\mathrm{T}}$, $\mathbf{I}_{\mathrm{nxmx3}}$
Spherical Vision	S2	Vision / multiple	Pasive	$\mathbf{I}_{\mathrm{nxmx3}}, \mathbf{J}_{\mathrm{nxmx3}}, \mathbf{K}_{\mathrm{nxmx3}}$
IMU	S3	Linear acceleration & angular velocity	Pasive	$\ddot{x}$, $\ddot{y}$, ω
GPS	S4	Position	Pasive	x, y, z
LIDAR	S5	Range	Active	δ_j, ϕ_{j}
Encoder	S6	Position	Pasive	v, s
Compass	S7	Angle	Pasive	θ
Ultrasonic Sonar	S8	Range	Active	δ
Binocular Multifunction	S9	Vision / Range	Pasive	$P=(x,y,z)^{T}$, $\mathbf{I}_{\mathrm{nxmx3}}, \mathbf{J}_{\mathrm{nxmx3}}$

Sensor S1 represents a binocular stereo sensor with maximal resolution of 1600 x 1200pixels, at 15fps (frames per second), with a baseline magnitude of 63mm. The sensor device S2 represents a ring of visual sensors, which are geometrically arranged as a cylindrical array set up as a multi-stereo system. It is compounded of three colour cameras connected through an IEEE-1394 port centralised to the SS computer host. Device S3 is a 2-DOF gyroscope, with a 2-axis accelerometer integrated. The S4 is a GPS receiver with USB interface, with an accuracy of 5m 2D RMS when WAAS is enabled. It uses a GPS protocol NMEA 0183 and SiRF binary as secondary protocol. The S5 is a LiDAR sensor device with a scanning area of 240°, angular resolution of 0.36°, and an

accuracy range from 60 – 4,095mm. Multiple S6 can be present in the SS, which are quadrature encoders with 90 pulses per revolution. Sensor S7 is a magnetic compass with accuracy of 0.5° and works with an I^2C interface. The S8 are ultrasonic sonar sensors ranging 100 – 5,000mm. S9 are two visual sensor calibrated as a stereo pair, but configured with an embedded vision processor. Both are set up to either work individually, or in combination as a binocular stereo sensor. Both visual sensors process colour images with resolution of 352 x 288 pixels. This manuscript mainly focuses on discussing how to provide a mathematical formulation for data registration deploying twelve devices: three S2, one S5 and eight S8. Although, S2 are in principle 2D images, a radial multi-stereo model is formulated in the present context. So that, 3D information inferred from S2 is then homogenised with S5 and S8. Furthermore, the SS is an apparatus that also poses a set of output ports to control eight (or more if expanded) actuator devices via pulse width modulation (PWM).

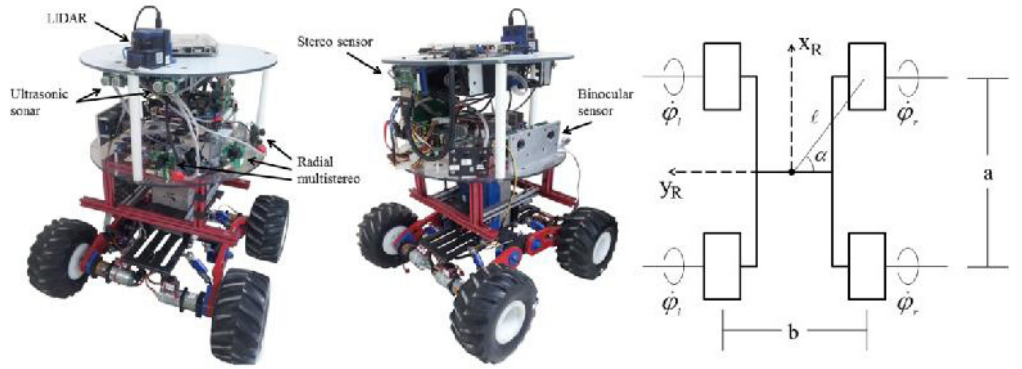

Fig. 1. Left and center: Wheeled mobile robot "Popeye" with a sensor suite on-board; right: platform kinematic model, configures as differential drive with 4 contact points.

3. Robot Position Model

To build global maps, a common inertial coordinate system must be defined. Each sensor obtains environmental attributes with different local Cartesian systems, even w.r.t. robot's local frame (see fig 2). Therefore, in the present work, twelve local coordinate systems are homogenised through homogeneous transformations. Data registration with different spatio-temporal sensing sources critically relay on accurate postures. Our study involves the deployment of a non-holonomic robotic platform, namely "Popeye" depicted at figure 1. At its right side, the robot's kinematic parameters are shown. The robot's speed Cartesian components X and Y are defined as a two asynchronous speeds (differential drive model), Data registration depends on robot's pose. The position and motions of a robotic platform must be modelled relaying on its kinematic restrictions, because they mathematically describe the geometry of movement of the robot in its surroundings, allowing us to know past present and future kinematic postures of the robot. Such information may be critically important for a registration data scheme. Thus, for a robot of two asynchronous velocities and four wheels (fig. 1) the first derivative posture model is given by,

$$\dot{x}_R(t) = \upsilon \cos\theta(t) \tag{1}$$

$$\dot{y}_R(t) = \upsilon \sin\theta(t) \tag{2}$$

and robot's orientation,

$$\dot{\theta} = \arctan\left(\frac{\dot{y}_R(t)}{\dot{x}_R(t)}\right) \tag{3}$$

In vector form, we define the input vector of the control system by **u**, with instantaneous tangential velocity, and angular speed,

$$\mathbf{u} = \begin{pmatrix} \upsilon(t) \\ \omega(t) \end{pmatrix} \tag{4}$$

One the **u** component is instantaneous absolute velocity $\upsilon(t)$, its model is approximated by an average of two asynchronous active wheels, so that,

$$\upsilon(t) = \frac{r}{2}\left(\dot{\varphi}_r + \dot{\varphi}_l\right) \tag{5}$$

The wheel's radius magnitude r is ideally the same for all wheels. Wheels instantaneous angular velocities are $\dot{\varphi}_r$ (right-sided wheels), $\dot{\varphi}_l$ and (left-sided wheels). In addition, the robot's angular velocity is a direct function of the wheels rotational speeds difference. Its angular behavior is consequently described by the differential magnitude of wheels speed [7]. Thus, the robot's global behavior given by its differential velocity is defined by $\hat{\upsilon}(t) = \upsilon_r - \upsilon_l$. The transversal differential speed component of the robot w.r.t. its geometric centre (ideally overlapping its centre of mass) is inferred by,

$$\omega(t) = \frac{\hat{\upsilon}(t)\cos(\alpha)}{\ell} \tag{6}$$

According to Fig. 1-right, ℓ is the distance between the robot's ideal centre of mass, and any wheel's contact point, with constant angle α. Algebraically substituting factors in order to state a new expression in terms of transversal and longitudinal metrics, $\ell = 0.5\sqrt[2]{\mathrm{a}^2 + \mathrm{b}^2}$. Then, the new equation to describe the robot's angular velocity in terms of contact points metrics, a and b, is given by,

$$\omega(t) = 2\mathrm{b}r\left(\dot{\varphi}_r - \dot{\varphi}_l\right)\left(\mathrm{a}^2 + \mathrm{b}^2\right)^{-1} \tag{7}$$

Therefore, the robot's pose model used to register non-stationary multi-sensor data is given by the recursive set of expressions [5-6],

$$\begin{pmatrix} x \\ y \\ \theta \end{pmatrix} = \begin{pmatrix} x_0 \\ y_0 \\ \theta_0 \end{pmatrix} + \begin{pmatrix} \int_t \left(\upsilon 0 + \int_t \dot{\upsilon}(t)\mathrm{d}t\right)\cos\left(\theta_0 + \int_t \left(\omega_0 + \int_t \dot{\omega}(t)\mathrm{d}t\right)\mathrm{d}t\right)\mathrm{d}t \\ \int_t \left(\upsilon 0 + \int_t \dot{\upsilon}(t)\mathrm{d}t\right)\sin\left(\theta_0 + \int_t \left(\omega_0 + \int_t \dot{\omega}(t)\mathrm{d}t\right)\mathrm{d}t\right)\mathrm{d}t \\ \int_t \left(\omega_0 + \int_t \dot{\omega}(t)\mathrm{d}t\right)\mathrm{d}t \end{pmatrix} \tag{8}$$

4. Sonar sensor

A sonar sensor is an electro-acoustic device that measures range of the nearest orthogonal point by using a time-of-flight ranging technique. Sensitivity range of an ultrasonic sonar ranges from 0.10m ≤ s < 5m. An ultrasonic sonar sensor is topically deployed in mobile robotics to measure range information. In this work, a ring of eight sonar sensors radially arranged were deployed in our robotic platform [9]. Given that, depth information w.r.t. environmental objects is measured through sound, we have that fundamentally the speed of sound in general is modelled by,

$$s = \frac{ct}{2} \tag{9}$$

where c is the sound speed; s is the distance an acoustic vibration travelled over an elapsed period of time t. Measurement data are treated by a homogeneous transformation to represent the environment in robot's fixed coordinate system, according to 2-a),

$$\mathbf{s}^R_{sonar_j} = l_j \begin{pmatrix} \cos(\phi_j) \\ \sin(\phi_j) \\ 0 \end{pmatrix} + d_j(t) \begin{pmatrix} \cos(\theta_j) \\ \sin(\theta_j) \\ 0 \end{pmatrix} \tag{10}$$

where $d_j(t)$ is the measurement value and l_j is considered as the Cartesian distance w.r.t. robot's geometric centre to the j^{th} sonar. ϕ_j is the angle of the distance l_j where the sonar is located. Angle θ_j is the orientation of the sonar (see fig. 2.a).

$$\mathbf{s}^{R}_{sonar_j} = \begin{pmatrix} l_j \cos\left(\phi_j\right) + d_j(t)\cos\left(\theta_j\right) \\ l_j \sin\left(\phi_j\right) + d_j(t)\sin\left(\theta_j\right) \\ 0 \end{pmatrix} \tag{11}$$

Further, by transforming onto a global Cartesian coordinate system for $\xi_t = (x, y, \theta)^{\cdot}$.

$$\mathbf{p}^{I}_{sonar_j} = \mathbf{R}\left(\gamma\right)\cdot\mathbf{s}^{R}_{sonar_j} + \xi_t \tag{12}$$

and substituting expression terms,

$$\mathbf{p}^{I}_{sonar_j} = \begin{pmatrix} \cos\gamma & -\sin\gamma & 0 \\ \sin\gamma & \cos\gamma & 0 \\ 0 & 0 & 1 \end{pmatrix} \cdot \begin{pmatrix} l_j \cos\left(\phi_j\right) + d_j(t)\cos\left(\theta_j\right) \\ l_j \sin\left(\phi_j\right) + d_j(t)\sin\left(\theta_j\right) \\ 0 \end{pmatrix} + \begin{pmatrix} x \\ y \\ \theta \end{pmatrix} \tag{13}$$

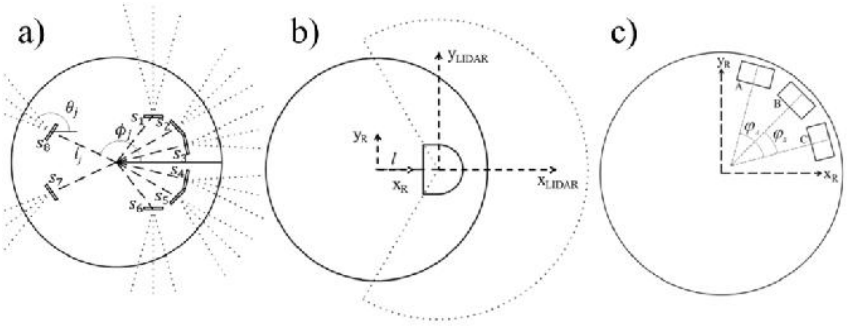

Fig. 2. a) Ultrasonic sonar configuration; b) LIDAR location and orientation; c) Radial multistereo system.

5. Light detection and range sensing model

Light detection and ranging (LIDAR) sensor is an electro-optical device deployed to measure range of points by electromagnetic signal time-of-flight technique. For a LiDAR sensor, range data are collected with cylindrical order, where points are referenced by distance and known bearing. We deployed a Hokuyo UBG-04LX-FO1, with a scanning area of 240°, and was configured with an angular resolution of 0.36°, which includes a range accuracy of 60-4,095mm. According to sensor position on-board the robotic platform, the LiDAR distance sensing model w.r.t. a common Cartesian reference for all k scanning points. See 2-b), where $\delta_i(t)$ is the i^{th} measurement range value. In addition, l is considered as the Cartesian distance w.r.t. robot's geometric centre to any LiDAR radial measurement (see fig. 2.b). Likewise, $\Delta\phi$ is the angular resolution, and ϕ_0 is the minimum angle in the scan.

$$\mathbf{s}^{R}_{\mathrm{LIDAR}} = \begin{pmatrix} \delta_i(t)\cos\left(\Delta\phi\left(i-1\right) + \phi^{\ell}_0\right) + l \\ \delta_i(t)\sin\left(\Delta\phi\left(i-1\right) + \phi^{\ell}_0\right) \\ 0 \end{pmatrix}_{i=1}^{k} \tag{14}$$

Thus, by transforming into a global inertial coordinate system, our homogeneous rigid roto-translation model,

$$\mathbf{p}'_{\mathrm{LIDAR}} = \mathbf{R}(\gamma)\cdot\mathbf{s}_{\mathrm{LIDAR}}{}_{i=1}^{k} + \xi_t \tag{15}$$

and substituting rotation and translation terms accordingly,

$$\mathbf{p}_{\mathbf{LIDAR}^{\cdot}}(t) = \begin{pmatrix} \cos\gamma & -\sin\gamma & 0 \\ \sin\gamma & \cos\gamma & 0 \\ 0 & 0 & 1 \end{pmatrix} \cdot \begin{pmatrix} \delta_i(t)\cos\left(\Delta\phi\left(i-1\right) + \phi^{\ell}_0\right) + l \\ \delta_i(t)\sin\left(\Delta\phi\left(i-1\right) + \phi^{\ell}_0\right) \\ 0 \end{pmatrix}_{i=1}^{k} + \begin{pmatrix} x \\ y \\ \theta \end{pmatrix} \tag{16}$$

6. Radial Multistereo System

In this section, we present a radial multi-stereo vision system. The term "radial" is because of the circular geometric arrangement of three or more visual sensors located w.r.t. a common Cartesian origin. A traditional stereo device system is a pairwise camera mechanically calibrated. A pair stereo system is used to obtain range information. The X-axis of both cameras are collinear (separated by a baseline distance namely *b*) and their Y-axis, and Z-axis are parallel [10]. After identifying a point at both images called data association process, the range of real object in the scene may be estimated by the disparity value in both cameras' frame. Disparity is the difference between X-coordinates in both, left and right images. The proposed radial multi-stereo system consists of three cameras radially distributed where the image planes are slightly overlapped. In addition, not only radial stereo, but panoramic images are obtained. The geometric scheme of a radial multistereo system (see figure 3), the relationship among the common convergence centre, camera B, and camera C, an isosceles triangle is formed.

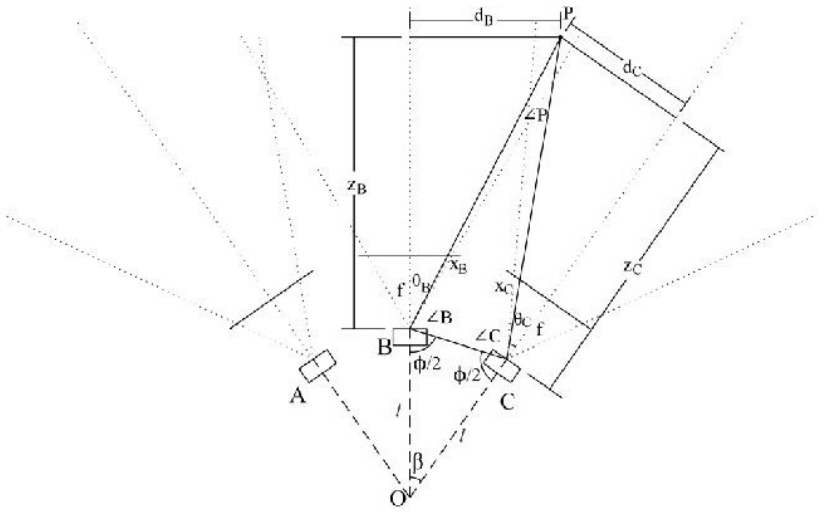

Fig. 3. Radial multistereo system.

Let us call β the angle between cameras B, and C. Therefore, angle ϕ is determined by summing inner triangle's angles, by $\beta+\phi=\pi$ and $\phi=\pi-\beta$. Hence, $\frac{\phi}{2}=\frac{\pi}{2}-\frac{\beta}{2}$. Thus, by applying sine's law, $\overline{\mathrm{BC}}$ is calculated, which is the linear distance from camera B to camera C. Likewise, *l* is the distance from O to any camera. Following the figure 3, the next relationship is stated,

$$\frac{\overline{\mathrm{BC}}}{\sin\beta}=\frac{l}{\sin\left(\frac{\phi}{2}\right)} \tag{17}$$

substituting the angle in right-side term, and by dropping-off the distance of interest,

$$\overline{\mathrm{BC}}=\frac{l\sin\beta}{\sin\left(\frac{\pi}{2}-\frac{\beta}{2}\right)} \tag{18}$$

The angle from the optical axis and the ray of projection of P at focal point of the camera B and camera C is calculated. X_B is the x-coordinate of the feature at the plane of camera B. x_C is the x-coordinate of the feature at the plane of camera C. f is the focal length of the camera.

$$\theta_B=\tan^{-1}\left(\frac{x_B}{\mathrm{f}}\right);\qquad \theta_C=\tan^{-1}\left(\frac{x_C}{\mathrm{f}}\right) \tag{19}$$

Besides, complementary angles models are stated,

$$\angle B = \frac{\pi}{2} - \theta_B + \frac{\beta}{2}; \qquad \angle C = \frac{\pi}{2} - \theta_C + \frac{\beta}{2} \tag{20}$$

Likewise, . $\angle P = \theta_B + \theta_C - \beta$ Thus, in order to estimate the range from cameras B and C w.r.t. point P, the linear distance from each camera in the radial system (B and C), to the point P is calculated by sine's law by,

$$\frac{\overline{\mathrm{BC}}}{\sin \angle P} = \frac{\overline{\mathrm{CP}}}{\sin \angle B}; \quad \text{and dropping-off } \angle\overline{\mathrm{CP}} \qquad \overline{\mathrm{CP}} = \frac{\overline{\mathrm{BC}} \sin \angle B}{\sin \angle P} \tag{21}$$

Hence, the model to express depth information is given by $z_B = \overline{\mathrm{BP}} \cos\theta_B$. Thus, by substituting $\overline{\mathrm{BP}}$ and θ_B, the model is more specified.

$$z_B = \left(\frac{\left(\frac{l \sin\beta}{\sin\left(\frac{\pi}{2} - \frac{\beta}{2}\right)} \right) \sin\left(\frac{\pi}{2} - \theta_C + \frac{\beta}{2}\right)}{\sin\left(\theta_B + \theta_C - \beta\right)} \right) \cos\left(\tan^{-1}\left(\frac{x_B}{\mathrm{f}} \right) \right) \tag{22}$$

In addition, and similarly the range between camera C and point P is defined by $z_C = \overline{\mathrm{CP}} \cos\theta_C$. Thus, substituting $\overline{\mathrm{CP}}$ and θ_C, it is defined.

$$z_C = \left(\frac{\left(\frac{l \sin\beta}{\sin\left(\frac{\pi}{2} - \frac{\beta}{2}\right)} \right) \sin\left(\frac{\pi}{2} - \theta_B + \frac{\beta}{2}\right)}{\sin\left(\theta_B + \theta_C - \beta\right)} \right) \cos\left(\tan^{-1}\left(\frac{x_C}{\mathrm{f}} \right) \right) \tag{23}$$

In addition, with depth models z_B and z_C, then real X-coordinates from the cameras B (d_B) and C (d_C) w.r.t. point P, can be estimated. Therefore, $d_B = z_B \tan\theta_B$, and

$$d_B = z_B \tan\left(\tan^{-1}\left(\frac{x_B}{\mathrm{f}} \right) \right); \qquad d_B = \frac{z_B x_B}{\mathrm{f}} \tag{24}$$

Likewise, because of $d_C = z_C \tan\theta_C$, and substituting,

$$d_C = z_C \tan\left(\tan^{-1}\left(\frac{x_C}{\mathrm{f}} \right) \right); \qquad d_C = \frac{z_C x_C}{\mathrm{f}} \tag{25}$$

Similarly, algebraic deduction is given for Y-Component and real Y-coordinates w.r.t point P using cameras B (h_B) and C (h_C), are given by,

$$\frac{h_B}{y_B} = \frac{z_B}{\mathrm{f}}; \qquad h_B = \frac{z_B y_B}{\mathrm{f}} \tag{26}$$

and,

$$\frac{h_C}{y_C} = \frac{z_C}{\mathrm{f}}; \qquad h_C = \frac{z_C y_C}{\mathrm{f}} \tag{27}$$

and the sensing model of camera C from pair of cameras B and C,

$$\mathbf{c}_{B,C}^{R}(t) = \begin{pmatrix} \frac{\left(\frac{\left(\frac{l \sin\beta}{\sin\left(\frac{\pi}{2} - \frac{\beta}{2}\right)} \right) \sin\left(\frac{\pi}{2} - \theta_B + \frac{\beta}{2}\right)}{\sin\left(\theta_B + \theta_C - \beta\right)} \right) \cos\left(\tan^{-1}\left(\frac{x_C}{\mathrm{f}} \right) \right) x_C}{\mathrm{f}} \\ \left(\frac{\left(\frac{l \sin\beta}{\sin\left(\frac{\pi}{2} - \frac{\beta}{2}\right)} \right) \sin\left(\frac{\pi}{2} - \theta_B + \frac{\beta}{2}\right)}{\sin\left(\theta_B + \theta_C - \beta\right)} \right) \cos\left(\tan^{-1}\left(\frac{x_C}{\mathrm{f}} \right) \right) \\ 0 \end{pmatrix} \tag{28}$$

Following for cameras A and B, their models are obtained by,

$$\mathbf{a}^{R}_{A,B}(t)=\begin{pmatrix}\dfrac{\left(\dfrac{l\sin\beta}{\sin\left(\frac{\pi}{2}-\frac{\beta}{2}\right)}\right)\sin\left(\frac{\pi}{2}-\theta_B+\frac{\beta}{2}\right)}{\sin\left(\theta_A+\theta_B-\beta\right)}\cos\left(\tan^{-1}\left(\dfrac{x_A}{\mathrm{f}}\right)\right)x_A\\ \mathrm{f}\\ \dfrac{\left(\dfrac{l\sin\beta}{\sin\left(\frac{\pi}{2}-\frac{\beta}{2}\right)}\right)\sin\left(\frac{\pi}{2}-\theta_B+\frac{\beta}{2}\right)}{\sin\left(\theta_A+\theta_B-\beta\right)}\cos\left(\tan^{-1}\left(\dfrac{x_A}{\mathrm{f}}\right)\right)\\ \varphi_A\end{pmatrix};\quad \mathbf{b}^{R}_{A,B}(t)=\begin{pmatrix}\dfrac{\left(\dfrac{l\sin\beta}{\sin\left(\frac{\pi}{2}-\frac{\beta}{2}\right)}\right)\sin\left(\frac{\pi}{2}-\theta_A+\frac{\beta}{2}\right)}{\sin\left(\theta_A+\theta_B-\beta\right)}\cos\left(\tan^{-1}\left(\dfrac{x_B}{\mathrm{f}}\right)\right)x_B\\ \mathrm{f}\\ \dfrac{\left(\dfrac{l\sin\beta}{\sin\left(\frac{\pi}{2}-\frac{\beta}{2}\right)}\right)\sin\left(\frac{\pi}{2}-\theta_A+\frac{\beta}{2}\right)}{\sin\left(\theta_A+\theta_B-\beta\right)}\cos\left(\tan^{-1}\left(\dfrac{x_B}{\mathrm{f}}\right)\right)\\ \varphi_B\end{pmatrix} \tag{29}$$

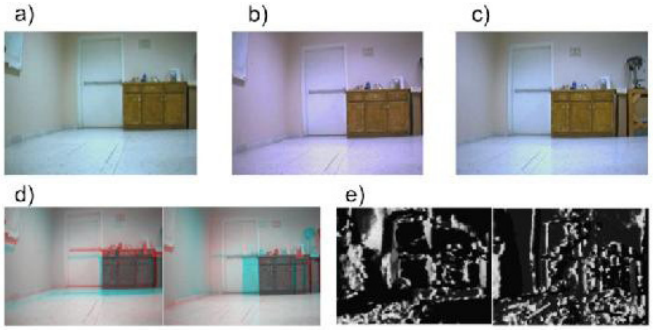

Fig. 4. Ring of multi-stereo sensors images (trinocular) rectified. A) image A; b) image B; c) image C; d) pairs of stereo images; e) disparity maps.

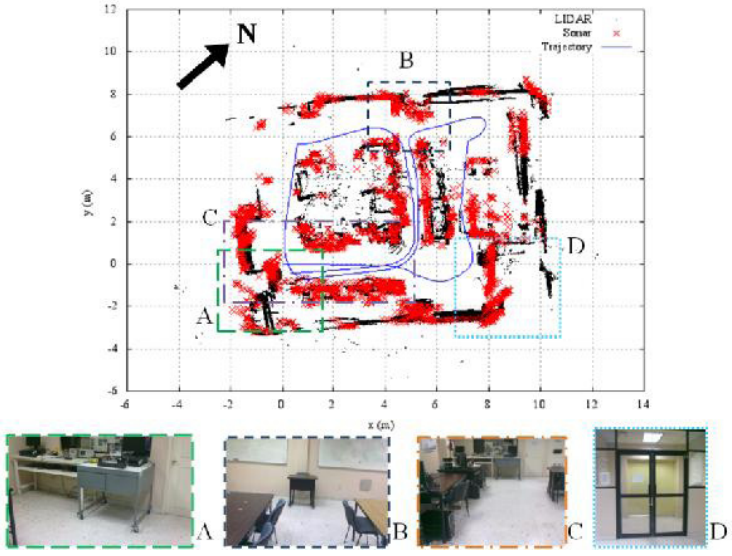

Fig. 5. Global map data registration using a ring of eight sonar, and a LiDAR.

7. Experimental Results

Indoor experimental results were carried out in the Laboratorio de Robótica at UACJ, in which such experiments consisted of tele-operated explorations within dynamic situations. The robotics platform “Popeye” was deployed and its velocity model was used to estimate and predict positions, as to match with real data. Besides, the robot was instrumented with the sensor suite, using only a ring of ultrasonic sonar, and the LiDAR sensor (240° of sensing angle). Along its navigation path, data registration was carried out on-line on a global map.

See experimental results in figure 5. Registered data on a global plane carried out on-line through the formulation presented in eq. 13 and 16. The general 3D data registration model consists of union of datasets within a global Cartesian space from sonars $\Sigma=\{\mathbf{p}_i^S\}$ where $\mathbf{p}_i^S = (x,y,h_S)^\intercal$, laser $\Lambda=\{\mathbf{p}_i^L\}$ where $\mathbf{p}_i^L = (x,y,h_L)^\intercal$, and trinocular radial stereo $X_{AB}=\{\mathbf{p}_i^{AB}\}$ and $X_{BC}=\{\mathbf{p}_i^{BC}\}$ where $\mathbf{p}_i^{AB} = (x,y,z)^\intercal$ and $\mathbf{p}_i^{BC} = (x,y,z)^\intercal$ respectively. h_S and h_L are sonar and LiDAR heights, respectively.

At this stage, data synthesis process has not been carried out, and we only considered a deterministic model to unify eight sonar sensors, one laser range finder scan of 681 measurements, and depth information of a trinocular circular stereo sensor, through, Thus, more specifically, the 3D heterogeneous registration model formulated in this manuscript is defined by,

$$M = S \bigcup L \bigcup C_{AB} \bigcup C_{BC} \tag{30}$$

8. Conclusions

The authors presented a mathematical model to register heterogeneous 3D data on-line through one equation. Registration was given deploying data from eight ultrasonic sonar, and one high data density LiDAR. The sensor devices in discussion are coordinated and synchronized by a home-made distributed sensor suite system. In addition, a model to fuse depth information from a semi-ring of three visual sensors was formulated. The three visual sensors were arranged along a cylindrical ring. All sensors were geometrically placed on-board a wheeled mobile robot platform, and data registration was carried out navigating indoors. A mathematical formulation for data registration was used to obtain experimental results on global mapping. Twelve local coordinate systems were homogenized through transformations of data with different spatio-temporal sensing sources. Because of a semi-circular trinocular stereo sensor, it was proposed a depth information model that automatically rectifies, and calibrates rings of images. Our study involved the experimental deployment of a non-holonomic four-wheel-drive robotic platform, configured as a 2WD only. The position and motions of the robotic platform were implicitly involved in our formulation for data registration. The robot's kinematic restrictions model described its geometry of movement allowing us to know past, present and future robot's postures, being critical for data registration. Experimental results proved that our approach is fast and feasible to implement on-line.

Acknowledgements

The authors would like to thank CONACyT financial support under scholarship No. 274239. In addition, authors also appreciate the support given in Laboratorio de Robótica by its members for their technical collaborations.

References

[1] Khaleghi, B., Khamis, A., Karray, F.O., S.N. Razavi, Multisensor data fusion: A review of the state-of-the-art, Information Fusion (2012).
[2] Luo, R.C., Multisensor Fusion and Integration: A Review on Approaches and Its Applications in Mechatronics, IEEE Transactions on Industrial Informatics, vol. 8(1), pp. 49-60, 2012.
[3] Martínez-García, E. A., Yoshida, T., Ohya, A. and Yuta, S., Multi-robot Communication Architecture for Human-guiding, Journal of Engineering Manufacture Part B, Vol. 219(1), pp. 183-190, 2005
[4] Berná-Martínez, J., Maciá-Pérez, F., Ramos-Morillo, H. and Gilart-Iglesias, V., Distributed Robotic Architecture based on Smart Services, IEEE Intl. Conf. on Industrial Informatics, pp. 480-485, 2006.
[5] Martínez-García, E. A., and Torres-Córdoba, R.,2012. Exponential Fields Formulation for WMR Navigation, Journal of Applied Bionics & Biomechanics, IOS press, vol. 9, pp. 375-397.
[6] Martínez-García, E. A., and Torres-Córdoba, R., 2010. 4WD skid-steer trajectory control of a rover with spring-based suspension, Intelligent Robotics and Applications, Springer, Lecture Notes in Computer Science, Vol. 6425.
[7] Lerín, E., Martínez-García, E. A., and Mohan, R.E., 2012. Design of an All-Terrain Autonomous Holonomic Rover, 8th Intl. Conf. on Intelligent Unmanned Systems.
[8] Mitchell, H. B. *Multi-sensor Data Fusion. An introduction.* Springer. 2007.

[9] Siciliano, B. and Khatib, O. *Springer Handbook of Robotics*. Springer. 2008.
[10] Shapiro, L.G. and Stockman, G.C. *Computer Vision*. Prentice Hall. 2001.
[11] Calafiore, G. and Bona, B. Constrained optimal fitting of three-dimensional vector patterns. IEEE Transactions on Robotics and Automation, 14(5):838-844, 1998.
[12] Carlone, L. and Bona, B. On registration of uncertain three-dimensional vectors with application to robotics. In Proceedings of the IFAC World Congress, 2011.
[13] Songmin Jia; Wei Cui; Xiuzhi Li; Jinhui Fan; Jinbo Sheng, "Mobile robot Bayesian map building based on laser ranging and stereovision," Computer Science and Automation Engineering (CSAE), 2011 IEEE International Conference on , vol.3, no., pp.308,312, 10-12 June 2011
[14] Moghadam, P.; Wijesoma, W.S.; Dong Jun Feng, "Improving path planning and mapping based on stereo vision and lidar," Control, Automation, Robotics and Vision, 2008. ICARCV 2008. 10th International Conference on , vol., no., pp.384,389, 17-20 Dec. 2008
[15] Thompson, S.; Kagami, S., "Stereo vision and sonar sensor based view registration for 2.5 dimensional map generation," Intelligent Robots and Systems, 2004. (IROS 2004). Proceedings. 2004 IEEE/RSJ International Conference on , vol.4, no., pp.3444,3449 vol.4, 28 Sept.-2 Oct. 2004.